Electron-wave dephasing suppressed by spin–orbit interaction in slightly hydrogenated graphene within a topological insulating regime

J. Kamijo[1], T. Nakamura[2], T. Kato[1], J. Haruyama[1*]

[1]Faculty of Science and Engineering, Aoyama Gakuin University, 5-10-1 Fuchinobe, Sagamihara, Kanagawa 252-5258, Japan

[2]Institute for Solid State Physics, The Tokyo University, 5-1-5 Kashiwanoha, Kashiwa, Chiba 277-8581, Japan

*Corresponding author E-mail: J-haru@ee.aoyama.ac.jp (J. H.)

Spin–orbit interaction (SOI) is known to scatter electron spin, causing spin flipping (dephasing in phase interference of electron waves) in thin metals, semiconductor two-dimensional (2D) electron gases, and carbon nanotubes. Thus, the introduction of SOI tends to eliminate the specific advantage of graphene for spintronics, which can retain spin phase stronger than other 2D materials because of absent SOI. Here, we report that Rashba-type SOI introduced by precise slight-hydrogenation of graphene can strongly suppress dephasing in interference phenomena, in contradiction to that in other 2D materials. This opens the door to novel carbon spintronics manifested by spin interference with SOI as a topological insulator.

The small mass of carbon atoms has prevented the experimental introduction of intrinsic spin–orbit interaction (SOI), which produces various interesting phenomena in graphene such as topological insulating states and the spin Hall effect (SHE)[1-6]. However, it was recently reported that the controlled addition of small amounts of covalently bonded hydrogen atoms (e.g., $N_H < 0.1\%$) can introduce a colossal enhancement of the SOI as a result of out-of-plane symmetry breaking (the so-called Rashba-type SOI), resulting in the SHE[7,8].

Phase interference of electron spin waves in two-dimensional (2D) materials is one of the attractive quantum effects within a diffusive carrier transport regime, and is highly valuable for spintronics (supplementary information (SI) (1))[11-17,26]. Weak localization (WL ; a constructive phase interference between two partial electron waves encircling a 2D plane in opposite directions along time-reversal symmetry paths[11-17,26]) is a typical phenomenon. In conventional 2D materials, SOI causes spin flipping and transforms WL to anti-localization (AL; a destructive phase interference) through a π phase shift[9,10]. Phenomena arising from phase interference have also been reported in SOI-absent graphene containing a large amount of adatoms (foreign atoms or defects) and ripples in the substrate[27-29]. For instance, a large magnitude of WL has been reported[27,28].

On the other hand, it has not been experimentally revealed how SOI affects phase interference in graphene because the realization of the coexistence of SOI with phase interference in graphene is difficult for the following reason. A heavy volume of adatoms (e.g., $N_H >> 0.1\%$) induces phase interference, while it tends to destroy SOI. In contrast, a slight amount of hydrogenation (e.g., $N_H < 0.05\%$) introduces SOI as mentioned above, but also causes less phase interference. Therefore, precise control and optimization of a small amount of N_H is crucial to produce the crossover N_H regime between these two regimes and clarify the correlation of SOI with phase interference phenomena.

Some recent theories have reported this correlation. For the out-of-plane mirror-symmetric SOI systems[9] of graphene with Berry phase[10] (β, with $\beta/\pi < 0.5$), SOI leads to the suppression of dephasing in the WL correction. SOI coupling with the in-plane Zeeman effect can also reduce this SOI-suppressed dephasing through sp^3 hybridization by asymmetrically deposited impurities[9]. These theories imply that the SOI-suppressed dephasing in topological insulating graphene are highly useful for future spintronic devices[18,19] because spin coherence can be maintained much more effectively, despite the presence of SOI and one can control spin through the SOI by applying electric fields as well as graphene edge spintronics[20-25].

In the present experiments, an electron beam (EB) dose, which precisely irradiated a hydrogen silsesquioxane (HSQ) resist ($(HSiO_{3/2})_n$) applied to pristine graphene, achieved an accurately

low-level hydrogenation ($N_H \ll 0.1\%$) of graphene, as optimized according to refs. 7 and 25 (SI (2)). The N_H estimated from the *D/G* peak ratios in Raman spectra (SI (2)) is linearly proportional to the EB dose (Fig. 1A). To introduce N_H values (e.g., ~ 0.06%) similar to those in ref. 7 that reported the introduction of colossal SOI (SI (2)), we employed EB doses which are approximately 10-times greater than those in ref. 7 due to differences in our EB facility. These EB irradiation doses introduced limited disorder (defects) only in some portions of the graphene surface. This induced phase interference phenomena, however, SOI could persist due to the low-level of N_H.

Figures 1B and 1C, respectively, show an optical microscope image and a schematic view of the four-probe electrode pattern used to detect phase interference phenomena of spin electron waves as changes in non-local resistance (R_{NL}) for hydrogenated (*H*)-graphene. As mentioned in Fig. 1C caption, the spin current due to SHE, driven from constant current flowing between electrodes 3 and 4 under applied back gate voltages (V_{bg}), accumulates in the area around electrodes 1 and 2, creating spin phase interference path (e.g., the loop-like constructive spin phase interference paths for WL). Indeed, resistance peaks, as shown in Fig. 2A, are not evidently observed in the local resistance measurement at electrodes 3 and 4 (SI (3)).

R_{NL} is shown as a function of V_{bg} and N_H in Fig. 2A. Three R_{NL} peaks around V_{bg} ~ 13, 22, and 28 V for $N_H = 0.06\%$ are clearly visible. In contrast, these R_{NL} peaks are not apparent for pristine graphene (i.e., $N_H = 0\%$ in Fig. 2A), in which only a very small R_{NL} peak due to ohmic contribution is observed around V_{bg} ~ 13 V[7]. As shown in Fig. 2B, only the R_{NL} peak around V_{bg} ~ 13 V increases significantly with increasing N_H in the low N_H region ($N_H < 0.03\%$).

In Fig. 2C, the in-plane-*B* dependence of the R_{NL} peak is shown for $N_H = 0.02\%$ of Fig. 2B. It exhibits an oscillatory behavior, which is an indication of SOI, as reported in ref. 7. In ref. 7, negative MRs were reported with an oscillatory behavior at the R_{NL} peaks over a range of in-plane *B*. As this behavior can be explained by the Larmor spin precession frequency ($\omega_B = \Gamma\Delta B \leq D_s/W^2$, where Γ is the gyromagnetic ratio, ΔB is the oscillation period, *W* is the width of the sample, and D_s is the spin diffusion coefficient), it provided a strong evidence for the presence of SOI and SHE. In ref. 7, the best fit to the oscillatory signal data in the ΔB range of ~8 T was observed for μ ~ 20,000 cm²V⁻¹s⁻¹ and $W = 1$ ($D_s \propto \mu$). On the other hand, our diffusive samples have low μ ($< $ ~10,000 cm²V⁻¹s⁻¹) and $W = 4$ μm, resulting in a D_s/W^2 value 30 times smaller than that reported in ref. 7. The ΔB range $< $ ~0.2 T in Fig. 2C satisfies the condition $\omega_B = \Gamma\Delta B \leq D_s/W^2$, assuming similar Γ values. Hence, it suggests Larmor spin precession and the presence of SOI as well, as in ref. 7.

The applied V_{bg} ~ 13 V for this R_{NL} peak corresponds to a V_{bg} for the Dirac point in local measurement (Fig. 2A, inset). This is in qualitative agreement with the R_{NL} peak arising from SOI observed in ref. 7. In contrast, the other two R_{NL} peaks were not evident, with a conventional Hall bar pattern, previously[7] and in our present *H*-graphene measurement. Thus, the two additional R_{NL} peaks are unique to the four-probe pattern measurement at high V_{bg} and for the crossover N_H ($0.03\% < N_H < 0.1\%$). Consequently, other origins for the R_{NL} peaks should become dominant at $N_H \gg$ 0.03% in addition to SOI.

To clarify the other origins, the temperature dependence of $(R_{NL})^{-1}$ was measured. Fig. 3A shows the result, which indicates a semi-logarithmic temperature dependence of non-local conductance ($G_{NL} = (R_{NL})^{-1}$) values for the three R_{NL} peaks of Fig. 2A. It highlights a linear relationship at high temperatures (above ~6 K), whereas G_{NL} saturates below ~6 K. These results are in good qualitative agreement with those observed for WL in CNTs[11], 2DEG, and thin metal films, and suggest that the three R_{NL} peaks in Fig. 2A can be attributed not only to SOI but also to WL. This suggests that the two R_{NL} peaks at 22 and 28 V appear only when the accumulated spin density arising from the SHE satisfies the optimal values to create a constructive interference loop-path for WL in *H*-graphene. The origin of this effect is also discussed later from the viewpoint of electron waves encircling *H*-graphene *n*-times (Fig. 4C).

However, the critical temperature (T_c) between the high and low temperature regions is significantly different from other 2D materials. The best fit to the linear-temperature dependence at high temperatures by the WL formula in Eq. (1)[11] gives $p = 4$ for $W = 4$ μm and $L = 24$ μm for the present *H*-graphene.

$$G(T) = G_o + \frac{e^2}{2\pi^2 \hbar} \frac{W}{L} \ln\left[1 + \left(\frac{T}{T_c(B, \tau_s)}\right)^p\right] \qquad (1)$$

The fitted p value suggests dephasing of spin phase interference by electron–electron interactions, as in multi-walled CNTs[11]. In contrast, T_c of ~6 K, for low-temperature saturation at $B = 0$ T, is considerably higher than that observed in CNTs (e.g., $T_c = 0.3$ K for $B = 0$ T[11]). In conventional 2D materials, the phase relaxation length ($L_\phi(T) = \sqrt{D\tau_\phi}$) is given by $\tau_\phi^{-1}(T) = \tau_{in}^{-1}(T) + 2\tau_s^{-1}$ (where D is the diffusion constant, and τ_ϕ, τ_{in}, and τ_s are the relaxation times for phase coherence, and inelastic and magnetic spin scattering, respectively). At $T > T_c$ for $\tau_{in}(T)^{-1} >> \tau_s^{-1}$, dephasing is dominated by inelastic scattering factors reflected in the p value, whereas at $T < T_c$ for $\tau_{in}(T)^{-1} << \tau_s^{-1}$, magnetic spin scattering (which is largely independent of temperature) dominates the dephasing. A T_c of as high as ~6 K suggests the presence of a larger τ_s^{-1} rate in conventional 2D materials. On the other hand, our graphene samples, which were mechanically exfoliated from graphite, contain no magnetic impurities, which we carefully checked by superconducting quantum interference devices (quantum design). Moreover, the R_{NL} peaks in Fig. 2A are strongly associated with SOI (Figs. 2B and 2C). Thus, the high T_c can be attributed to the SO scattering rate τ_{so}^{-1}, rather than τ_s^{-1}. This implies that SOI suppresses dephasing arising from electron-electron interaction at high temperatures. Indeed, T_c increases with increasing N_H (i.e., increasing SOI), as shown in the inset of Fig. 3B. Even SOI length (L_{so}) as small as ~ 40 nm at $T = T_c$ ~ 6 K can be estimated from the temperature dependence under the high $B = 7$T in Fig.3A (SI (4)). Moreover, the presence of only positive conductance at low temperatures in Fig. 3A suggests the absence of AL and, hence, supports the theory that SOI does not cause spin flipping.

The application of perpendicular B to the graphene plane directly demonstrates dephasing and reconfirms the abovementioned SOI-suppressed dephasing in WL and the absence of spin flipping (i.e., absence of AL). With a perpendicular B, negative MRs for the R_{NL} peak at V_{bg} ~22 V of $N_H = 0.06\%$ and 0.1% samples are observed around $B = 0$ at T = 1.5 K, as shown in Fig. 4A, which is within the low temperature regime ($< T_c = 6$ K) for SOI-suppressed dephasing in Fig. 3A. Because the negative MR denotes a decrease in MR by dephasing caused by increasing B, it indicates the presence of WL (i.e., absence of spin flipping and AL) at $B = 0$, even under SOI. This is consistent with Fig. 3. Based on Fig. 3, the SOI should suppress dephasing in the WL under a perpendicularly applied B. As shown by the black symbols of Fig. 3B, the MR amplitude in WL decreases with increasing N_H, whereas the MR peak value at negative MR increases (white symbols). This strongly suggests that the induced SOI suppresses dephasing in WL as N_H increases. Indeed, the black dotted curve in Fig. 4A calculated from the theory of SOI-suppressed dephasing using L_{so} as small as ~40 nm (i.e., strong SOI obtained from Fig. 3A) shows good agreement with the experimental results (SI (5)). In contrast, the blue dotted curve obtained using L_{so} ~ 4 µm (i.e., weak SOI) exhibits a significantly sharper trend and deviates from the experimental results. These results strongly support SOI-suppressed dephasing in WL[10].

Importantly, these negative MRs are observed only in the three R_{NL} peaks shown in Fig. 2A. They are not observed for the other V_{bg}'s (SI (6)). This strongly supports the argument that the three R_{NL} peaks only appear at specified V_{bg}'s, for which the accumulated spin densities satisfy the conditions required to form constructive phase interference paths for WL.

Figure 4B shows negative MRs observed around three R_{NL} peaks at $T = 1.5$ K when an in-plane B is applied (SI (6)). The behavior is approximately linear and different from the oscillatory behavior due to SOI in low N_H region (<0.03 %), as shown in Fig. 2C. Only when $V_{bg} = 22$ V, an oscillatory-like behavior is observed with a period of ΔB ~ 4 T, which is only half of the ΔB range of 8 T, reported in ref. 7. As mentioned for Fig. 2C, our diffusive samples have low μ and $W = 4$ µm, leading to a D_s/W^2 value 30 times smaller than that in ref. 7. Thus, the ΔB range of ~4 T cannot satisfy the condition $\omega_B = \Gamma \Delta B \leq D_s/W^2$, assuming similar Γ values, and cannot be interpreted in terms of Larmor spin precession. Consequently, the Larmor spin precession observed in Fig. 2C is not the dominant factor in Fig. 4B.

3

Because WL is dominant in this N_H region, the linear relationships should be associated with the interplay between SOI and WL, which suppresses dephasing. It can be understood by the reduction of the SOI-suppressed dephasing in WL, when B is applied in-plane, as follows. An applied in-plane B conventionally causes no dephasing in spin phase interference and should lead to no MR changes. On the other hand, ref. 9 predicted that SOI-induced suppression of the dephasing in WL can be reduced by a decrease in SOI due to its coupling with the in-plane Zeeman effect, which depends linearly on the in-plane B. In our samples, the dephasing is suppressed even at $B = 0$ and T < 6 K (Fig. 3A). Thus, the MR values given by SOI-suppressed dephasing at $B = 0$ at T = 1.5 K linearly decrease by the dephasing recovered through an increase in in-plane B, resulting in the observed negative MRs with linear slope. The red dotted lines in Fig. 4B are fit to the experimental data by this theory[9], which actually gives a good fit. Consequently, the in-plane B dependence also supports the presence of SOI-suppressed dephasing at $B = 0$ T.

In the analysis for Fig. 4A, we focused on the negative MRs only around $B = 0$. On the other hand, when a higher perpendicular B is considered for ±5T, evident periodic MR oscillations are observed, as shown in Fig. 4C, limited only to the three R_{NL} peaks. These oscillations can be well-fitted by the theory of Altshuler-Aronov-Spivak (AAS) oscillations[12-17] with a constant normalised period $\Delta B \propto (1/2)(h/e)$, where h is the Planck's constant and e is the elemental charge of the electron (SI (1, 7)). This suggests that the SOI-suppression of dephasing in WL is quite significant even at high B because the phase interference path for AAS oscillation can exist only in tube-like structures in conventional materials and disappears as a result of dephasing caused by high B in conventional 2D materials.

Moreover, we find that the oscillation period ΔB among the three R_{NL} peaks decreases by a factor of two after each V_{bg} increase ($\Delta B = 8$, 4, and 2 T for $V_{bg} = 13$, 22, and 28 V, respectively; see inset of Fig. 4C). This suggests the presence of the AAS effect, arising from n-times-encircling paths around the AAS loop ($n = 1-3$; WL loop, as shown in Fig. 1C)[14], which is characterized by $\Delta B \propto (1/2)^n(h/e)(\pi r^2)^{-1}$ [14], as confirmed by fitting the data with the AAS theory. Because the AAS loop at $V_{bg} = 13$ V (corresponding to the Dirac point) is the most stable, the electron spins tend to circulate two- and three-times along the same AAS loop at the other two specified V_{bg}'s (i.e., 22 and 28 V) when a perpendicular B is applied. This can explain the three R_{NL} peaks that only appear at specified V_{bg}'s satisfying conditions appropriate for forming the WL path, and hence the AAS path with n-times encircling electron waves, as in the present case. Furthermore, even possible universal conductance fluctuations with SOI-suppressed dephasing are also observable in the present H-graphene (SI (8))[26].

References and Notes

1. Sinova, J. et al., *Phys. Rev. Lett.* **92** 126603 (2004).
2. Murakami, S., Nagaosa, N. and Zhang, S.C., *Science* **301,** 1348 (2003).
3. Castro Neto, A. H. and Guinea, F., *Phys. Rev. Lett.* **103**, 026804 (2009).
4. Kane, C. L. & Mele, E. J., *Phys. Rev. Lett.* **95**, 146802 (2005).
5. Kane C. L. & Mele, E. J., *Phys. Rev. Lett.* **95**, 226801 (2005).
6. Abanin, D. A., Geim, A. *et al.*, *Science* **332**, 328-330 (2011).
7. Balakrishnan, J., Koon, G. K. W., Jaiswal, M, Castro Neto, A. H. & Özyilmaz, B., *Nature Physics* **9**, 284-287 (2013).
8. Melinda, S. R., Kim, P. *et al.*, *Nano Lett.* **8**, 4597 (2008).
9. McCann E. and Fal'ko, V. I., *Phys. Rev. Lett.* **108**, 166606 (2012).
10. Shan, W.-Y. *et al.*, *Phys. Rev.* B **86** 125303 (2012).
11. Langer, L., Bayot, V., Grivei, E. and Issi, J.-P., *Phys. Rev. Lett.* **76**, 479 (1996).
12. She, S. H. *et al.*, *Phys. Rev. Lett.* **84**, 4441 (2000).
13. Song S.N. *et al.*, *Phys. Rev. Lett.* **72**, 697 (1994).
14. Bachtold A. *et al.*, *Nature* (London) **397**, 673 (1999).
15. Haruyama, J., Takesue, I. and Hasegawa, T., *Phys. Rev.* B **65**, 033402 (2001).
16. Altshuler, B.L. *et al.*, *JETP Lett.* **35**, 588 (1982).
17. Imry, Y., Introduction to mesosopic physics. (Oxford University Press, Oxford 2002)
18. Tombros N. *et al.*, *Phys. Rev. Lett.* **101**, 046601 (2008).
19. Tombros, N. *et al.*, *Nature* **448**, 571 (2007).
20. Hashimoto, T., Haruyama, J., Roche, S. *et al.*, In-depth review, *Nature Nanotech* (2014).
21. Tada, K., Hashimoto, T., Haruyama, J., Yang, H. & Chshiev, M. S, *Phys. Status Solidi B* **249**, 2491-2496 (2012).
22. Shimizu, T., Nakamura, J., Tada, K., Yagi, Y. & Haruyama, J., *Appl. Phys. Lett.* **100**, 023104 (2012).
23. Hashimoto, T., Kamikawa, S., Yagi,Y. & Haruyama, J., *Materials Sciences and Applications* **5**, 1-9 (2014).
24. Shimizu, T., Haruyama. J. *et al.*, *Nature Nanotech.* **6,** 45-50 (2011).
25. Kato, T., Nakamura, T., Haruyama. J. *et al.*, *Appl. Phys. Lett.* **104**, 252410 (2014).
26. Ando. T. et al., Mesoscopic physics and electronics. Nano Science and Technology series (Klitzing v. K. & Weisendanger R.), ISBN 3-540-63587-4 (Springer-Verlag 1998)
27. M. B. Lundeberg, R. Yang, J. Renard, and J. A. Folk, *Phys. Rev. Lett.* **110**, 156601 (2013)
28. M. B. Lundeberg et al., *Phys. Rev. Lett.* **105**, 146804 (2010)
29. M. B. Lundeberg et al. *Nature Physics* **5**, 894 (2009)
30. The authors thank S. Katsumoto, M. Yamamoto, S. Tarucha, M. Ezawa, H. Shinohara, H. Hibino, T. Ando, T. Enoki, B. Ozyilmaz, A. H. Castro Neto, S. Roche, and M. S. Dresselhaus for their technical contribution, fruitful discussions, and encouragement. The work at Aoyama Gakuin was partly supported by a Grant-in-aid for Scientific Research (Basic research A: 24241046) in MEXT and AOARD grant (135049) in U.S. Air Force Office of Scientific Research.
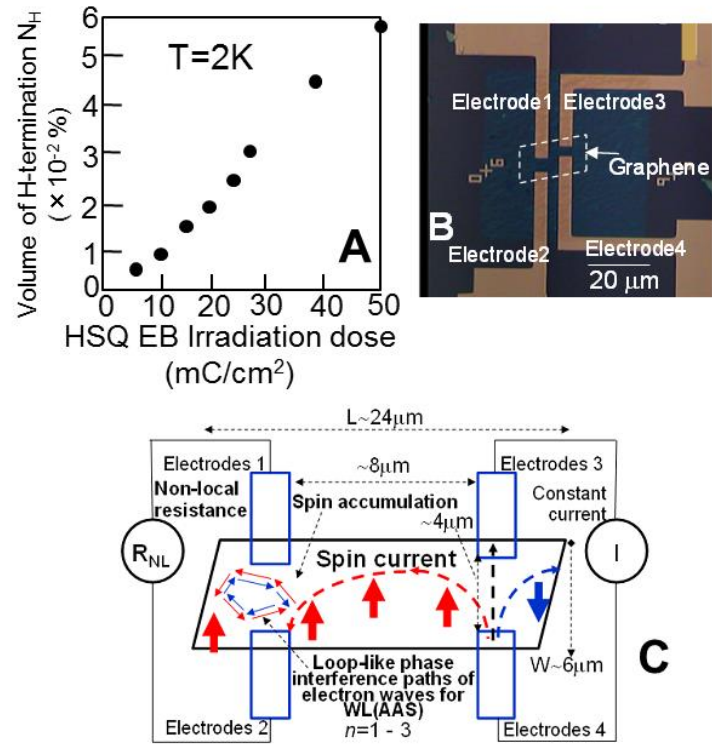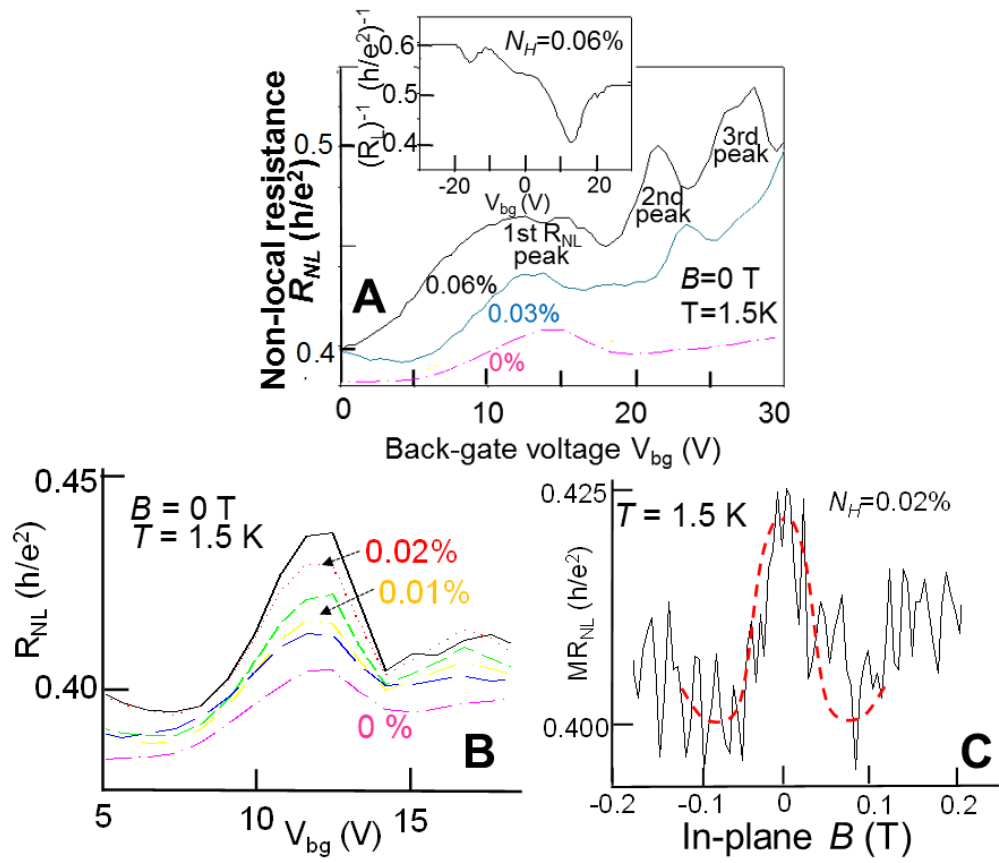
Volume of H-termination N_H ($\times 10^{-2}$ %)

T=2K

HSQ EB Irradiation dose (mC/cm^2)

A

Electrode1 Electrode3

Graphene

B

Electrode2 Electrode4

20 μm

L~24μm

Electrodes 1

Non-local resistance

~8μm

Spin accumulation

~4μm

Electrodes 3

Constant current

R_{NL}

Spin current

I

Loop-like phase interference paths of electron waves for WL(AAS) n=1 - 3

W~6μm

C

Electrodes 2

Electrodes 4
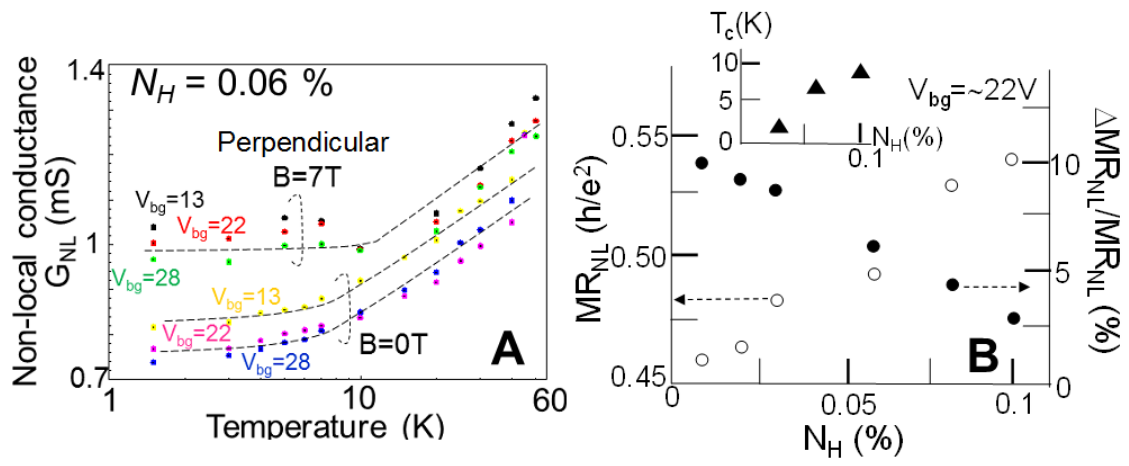
Figure 1
Haruyama et al.

Figure 2
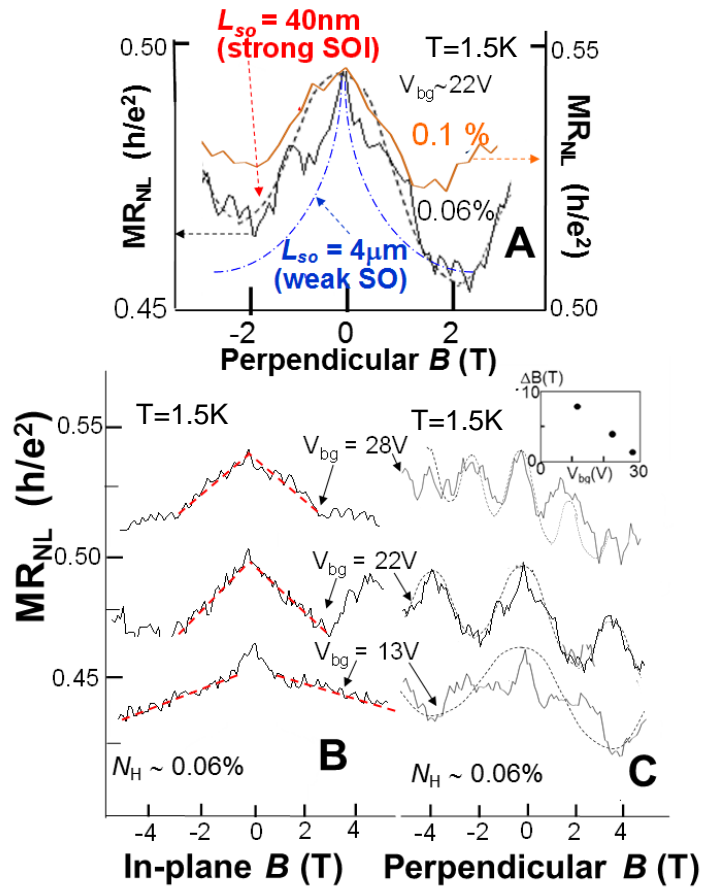Haruyama et al.

Figure 3
Haruyama et al.

Figure 4
Haruyama et al.

Figure captions

Fig. 1
(A) Volume (area) of N_H estimated from *D/G* peak ratios in the Raman spectra as a function of electron beam (EB) dose irradiated to the HSQ resist (SI (2)). EB irradiation doses (e.g., 50 mC/cm^2), which are employed in the present experiments to give the same N_H (e.g., ~0.06%) as those in ref. 7, are approximately ten-times larger than those in ref. 7 owing to differences in the EB facility. This leads to a slightly diffusive charge transport regime due to limited disorder in the present graphene with the maintenance of high quality and SOI.

(B) Optical microscope image of the four-probe electrode pattern on hydrogenated graphene.

(C) Schematic view of (**B**) with electron spin trajectories for SHE. In contrast to a conventional Hall bar, the two electrodes that make the main current flow were eliminated. When a constant current flows between electrodes 3 and 4 under V_{bg}, spin current due to the SHE(SOI) flows towards electrodes 1 and 2, and is confined and accumulated around these electrodes. This accumulation induces the formation of loop-like spin phase interference paths of electron waves for WL, which are detected as a change in R_{NL}.

Fig. 2
(A) R_{NL} as a function of V_{bg} and N_H (0, 0.03, and 0.06%). Only when N_H is 0.06%, three R_{NL} peaks are evident around V_{bg} ~ 13, 22, and 28 V. These were reconfirmed in at least in three samples. **Inset:** Local two-probe conductance measurement $[(R_L)^{-1}]$ (between electrodes 3 and 4 in Fig. 1C) as a function of V_{bg}.

(B) R_{NL} peak around V_{bg} ~ 13V, from (A), as a function of N_H in the low N_H region ($N_H < 0.03\%$).

(C) In-plane *B* dependence of the R_{NL} peak for $N_H = 0.02\%$ from (B).

Fig. 3
(A) Semi-logarithmic temperature dependence of the inverse values of the three R_{NL} peaks of Fig. 2A at perpendicular $B = 0$ and 7 T. They exhibit linear relationships at high temperatures ($> T_c$ ~6 K), whereas they saturate below T_c ~6 K. They are well accounted for by the WL theory (Eq. (1)) shown by dashed lines. These behaviors are observed only around the three R_{NL} peaks.

(B) R_{NL} peak values at B = 0 (white symbols for left Y-axis) and MR amplitude, $\Delta MR_{NL}/MR_{NL}$ (B = 0), (black symbols for right Y-axis) in WL as a function of N_H. ΔMR_{NL} is defined as the difference in MR peak and bottom values in individual N_H samples (see Fig. 4A).
Inset: T_c of (A) as a function of N_H.

Fig. 4
(A) Perpendicular-*B* dependence of the R_{NL} around V_{bg} ~ 22 V in the low *B* region for $N_H = 0.06\%$ and 0.1% samples. The dotted curves are data fits by the AAS theory using strong and weak SOI parameters ($L_{so} = 40$ nm and 4 μm, respectively) (SI (5)).

(B) In-plane-*B* dependence of the three R_{NL} peaks for $N_H = 0.06\%$ of Fig. 2(A). The dotted lines represent data fits by the theory for linear reduction of the SOI-suppressed dephasing by the coupling between SOI and the in-plane Zeeman effect[9].

(C) Perpendicular *B* dependence of the three R_{NL} peaks of Fig. 2A in the high *B* region. The periodic MR oscillations in the high *B* region are well described by the dashed curves, representing best fits

by the AAS theory performed with $L_{so} = 40$ nm, despite the 2D structure of graphene (SI (5)).

Inset: AAS oscillation period ΔB estimated at three different V_{bg}'s shown in the main panel. Their halving with increasing V_{bg} suggests the presence of n-times ($n = 1–3$) encircling electron waves along the WL path shown in Fig. 1C.